# Synergistic effect of repulsive inhibition in synchronization of excitatory networks

Igor Belykh, Reimbay Reimbayev, and Kun Zhao
*Department of Mathematics and Statistics and Neuroscience Institute, Georgia State University, 30 Pryor Street, Atlanta, Georgia 30303, USA*
(Received 9 August 2014; revised manuscript received 8 June 2015; published 29 June 2015)

We show that the addition of pairwise repulsive inhibition to excitatory networks of bursting neurons induces synchrony, in contrast to one's expectations. Through stability analysis, we reveal the mechanism underlying this purely synergistic phenomenon and demonstrate that it originates from the transition between different types of bursting, caused by excitatory-inhibitory synaptic coupling. This effect is generic and observed in different models of bursting neurons and fast synaptic interactions. We also find a universal scaling law for the synchronization stability condition for large networks in terms of the number of excitatory and inhibitory inputs each neuron receives, regardless of the network size and topology. This general law is in sharp contrast with linearly coupled networks with positive (attractive) and negative (repulsive) coupling where the placement and structure of negative connections heavily affect synchronization.

DOI: 10.1103/PhysRevE.91.062919 PACS number(s): 05.45.Xt, 87.19.L–

## I. INTRODUCTION

Synchrony has been broadly observed in pathological brain states, especially during epilepsy and Parkinson's tremors [1,2]. Epilepsy is characterized by two behaviors, short bursts of synchronized neuronal activity and long events called seizures [2]. There has been much work on the emergence of bursting rhythms in isolated and coupled neurons [3–6]. Coupled bursting neurons can exhibit different forms of synchrony: spike synchronization; burst synchronization, when only the envelopes of the spikes synchronize; complete synchrony; and antiphase bursting [7–9]. Excitatory and inhibitory connections often play opposite roles in inducing synchronization or antiphase bursting [7–22].

Fast nondelayed inhibition is known to promote pairwise antiphase synchronization in purely inhibitory networks [13]; whereas fast excitation induces synchrony as long as the coupling exceeds a threshold value [7–10]. Slow or time-delayed inhibitory and excitatory synapses reverse their roles such that slow or delayed inhibitory connections favor neural synchrony [14–17]. At the same time, synchronization in a pair of reciprocally coupled neurons with fast nondelayed inhibitory neurons is typically unstable. More specifically, it has been shown that fast nondelayed inhibition is always repulsive in the two-coupled network of *spiking* (nonbursting) cells [16], unless each cell has at least two slow intrinsic variables [17]. Recently, it was shown that fast nondelayed reciprocal inhibition can promote synchrony in some *bursting* cells such as the leech heart interneuron model and Purkinje neuron model, provided that the inhibitory connections are weak and the initial conditions are chosen close enough, within the spiking phase of bursting [18]. However, this synchronous rhythm has a small basin of attraction and is fragile and largely dominated by a much stronger coexisting antiphase bursting.

The network architecture also plays an important role in synchronization of an inhibitory network. For example, it was shown that even weak common inhibition of a bursting network with strong repulsive inhibitory connections by an external pacemaker neuron can induce synchronization within the network. This common inhibition can win out over the much (e.g., 100 times) stronger repulsive connections, provided that the pacemaker's duty cycle, the fraction of the period during which the neuron bursts, is sufficiently long [19]. Inhibitory connections also play various roles in the emergence of synchronous and asynchronous rhythms in neuronal motifs [20–24]. For example, the presence of a single reciprocally connected pair provides dynamical relaying in neuronal motifs that yields zero-lag synchrony despite long conduction delays [23,24].

In this paper we report a counterintuitive find that fast nondelayed *repulsive* inhibitory connections can robustly promote synchronization when added to an excitatory network of square-wave bursting neurons. This synergistic effect is caused by the ability of inhibition to effectively switch the type of network behavior from square-wave [4] to plateau ("tapered") bursting [5,25]. Square-wave bursting [3] was named after its shape during a burst which resembles a square wave. Plateau (tapered) bursting is characterized by spikes of decreasing size that turn into a plateau towards the end of the active phase of bursting [5]. Square-wave bursters are difficult to synchronize [7] and their spike synchronization requires strong excitatory coupling, whereas plateau bursters with smaller spikes are more prone to synchrony. The added inhibition causes plateau bursting so weaker excitatory coupling is sufficient to induce synchrony in the excitatory-inhibitory network. This effect is generic and observed in different models of bursting neurons. In this study, we choose the Hindmarsh-Rose neuron model as an individual unit of the network. It is important to emphasize that pairwise fast nondelayed inhibition is always repulsive in networks of Hindmarsh-Rose neurons, regardless of coupling strength and initial conditions. Yet its addition lowers the synchronization threshold much more significantly than strengthening the present excitatory connections due to the combined action of excitatory-inhibitory synaptic coupling and switching to plateau bursting.

While many studies use reduced neuronal models such as phase or relaxation oscillators where the spikes are ignored, our results promote the use of the detailed biophysical models, taking into account neuronal spikes and bursts. The discovered synergistic effect is due to nonlinear interactions of spikes; as a result, it is not observed in networks of the reduced models. Yet, there is experimental evidence that the onset and self-termination of seizures is accompanied by the transition

 

between different types of network bursting activities [6,26] where the spikes play an important role. Remarkably, the transition to abnormal synchrony corresponds to switching to plateaulike bursting [6].

We use the stability analysis to reveal the general mechanism of the induced synchronization and demonstrate that there is an optimal balance between the excitatory and inhibitory couplings that trigger synchronized bursting. These results are applicable to synchronization in a pair of connected neurons as well as to large networks with mixed excitatory-inhibitory connections. We discover universal scaling laws for the onset and loss of stable synchronization where the synchronization conditions are fully controlled by the number of excitatory and inhibitory inputs each neuron receives, regardless of the network size and topology. The independence of the synchronization conditions in purely excitatory networks of bursting neurons from the details of network architecture, except for the in-degree of each neuron, was reported in Ref. [9]. In this work, we show that the inhibition-induced synchrony is also controlled by the number of inhibition inputs to each neuron; however, the scaling law for the synchrony loss differs and involves a ratio of excitatory and inhibitory inputs. These general laws drastically differ from those in linearly coupled networks with positive (attractive) and negative (repulsive) coupling where the synchronization conditions are controlled by the structure of negative connections via the eigenvalues of the corresponding Laplacian matrix [27–29].

The layout of this paper is as follows. First, in Sec. II, we present and discuss the network model. In Sec. III, we report the main effect observed in a two-cell network with excitatory and inhibitory connections. We also discuss the details of the transition from square-wave to plateau bursting which is caused by the disappearance of a homoclinic bifurcation that governs the type of synchronized bursting. In Sec. IV, we derive the variational equations for the stability of the synchronous solution and explain the main synchronization mechanism. We also suggest the universal scaling laws for the stability of synchronization in large networks. In Sec. V, a brief discussion of the obtained results is given. Finally, the Appendix gives additional support to the scaling law, controlling the loss of synchrony caused by overly strong inhibition.

## II. THE MODEL AND PROBLEM STATEMENT

We consider a network of $n$ bursting Hindmarsh-Rose neuron models with excitatory and inhibitory connections:

$$\begin{aligned}\dot{x}_i &= ax_i^2 - x_i^3 - y_i - z_i + g_{\rm exc}(V_{\rm exc} - x_i)\sum_{j=1}^{n} c_{ij}\Gamma(x_j)\\ &\quad + g_{\rm inh}(V_{\rm inh} - x_i)\sum_{j=1}^{n} d_{ij}\Gamma(x_j),\\ \dot{y}_i &= (a+\alpha)x_i^2 - y_i, \quad \dot{z}_i = \mu(bx_i + c - z_i),\\ i,j &= 1,\ldots,n.\end{aligned} \tag{1}$$

Here $x$ represents the membrane potential, and variables $y$ and $z$ take into account the transport of ions across the membrane through fast and slow ion channels, respectively. The fast synaptic coupling is modeled by the sigmoidal function $\Gamma(x_j) = 1/[1+\exp\{-\lambda(x_j - \Theta_s)\}]$ [11] with the synaptic threshold $\Theta_s = -0.25$ [9]. The reversal potentials $V_{\rm exc} = 2 > x_i(t)$ and $V_{\rm inh} = -2 < x_i(t)$ for any $x_i$ and any $t$, i.e., the synapses are excitatory and inhibitory, respectively. Hereafter, the parameters are chosen and fixed as follows: $a = 2.8$, $\alpha = 1.6$, $\lambda = 10$, $c = 5$, $b = 9$, $\mu = 0.001$ [9,10]. The connectivity matrices $C = (c_{ij})$ and $D = (d_{ij})$ define the structure of excitatory and inhibitory connections, respectively; both mutual and unidirectional coupling are allowed. $g_{\rm exc}$ and $g_{\rm inh}$ are the corresponding synaptic strengths. It is required that all row-sums of $C$ and $D$ are equal to $k_{\rm exc}$ and $k_{\rm inh}$, the property that implies a network where each cell has $k_{\rm exc}$ inputs from excitatory neurons and $k_{\rm inh}$ from inhibitory ones. This constraint is chosen to ensure the existence of complete synchrony and to allow the use of the stability conditions to reveal the synchronization mechanism. Note that the dynamics of completely synchronized neurons differs from that of an isolated cell and is governed by the self-connected system:

$$\begin{aligned}\dot{x} &= ax^2 - x^3 - y - z + k_{\rm exc}\, g_{\rm exc}(V_{\rm exc} - x)\Gamma(x)\\ &\quad + k_{\rm inh}\, g_{\rm inh}(V_{\rm inh} - x)\Gamma(x),\\ \dot{y} &= (a+\alpha)x^2 - y, \quad \dot{z} = \mu(bx + c - z).\end{aligned} \tag{2}$$

This property is a key ingredient of the synergistic effect reported in this paper.

## III. TWO-CELL NETWORK: INHIBITION-INDUCED SYNCHRONIZATION

We start off with the simplest network where two cells (1) are symmetrically coupled through both excitatory and inhibitory connections with $k_{\rm exc} = 1$ and $k_{\rm inh} = 1$. From a neuroscientist's perspective, such a network can be viewed as the interaction between two excitatory neurons with direct excitatory and tertiary synapses [30] where the latter excites the presynaptic terminal of an inhibitory interneuron, allowing inhibition of the other excitatory cell (see Fig. 1) [31]. For delayed synapses, however, the dynamics might look different. From a physicist's perspective, this is a network of two pulse-coupled oscillators with attractive and repulsive connections.

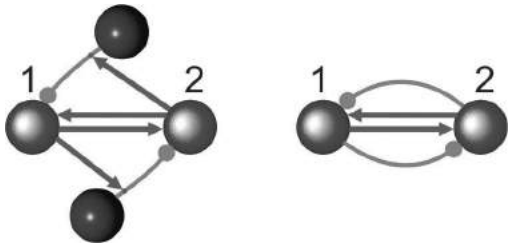


FIG. 1. (Color online) (Left) Possible interactions between two excitatory neurons 1 and 2 with direct excitatory and tertiary synapses. The tertiary synapses mediate inhibition by exciting the presynaptic terminals of inhibitory interneurons at their somas. This network can be viewed as a pair of neurons effectively coupled through both excitatory and inhibitory connections (right). Excitatory (inhibitory) connections are depicted by arrows (circles). The dynamics of the two-cell network is studied in Fig. 2.

We use this two-cell network to demonstrate the synergistic effect and clearly describe its stability mechanism. We will then show that the same results carry over to larger networks whose architecture always supports Dale's law [32] such that synaptic (outgoing) connections from a neuron to other cells are either all excitatory or inhibitory.

Figure 2 reveals that there is a broad interval of inhibitory strengths over which the repulsive inhibition compliments attractive excitation in promoting neural synchrony. Notice that the onset of spike (complete) synchronization through boundary $E1$ is accompanied by or close to the transition from square-wave to plateau bursting, indicated by the curve HB. The two curves practically coincide up to the values of $g_{\rm exc} \approx 0.8$ such that a significant reduction of the synchronization threshold for $g_{\rm exc}$ as much as 10 times, observed at the lower values of $g_{\rm exc}$ is governed by this transition between the two types of bursting. This transition occurs in both the purely excitatory [Fig. 2(b)] and mixed excitatory-inhibitory connections [Fig. 2(c)]. The addition of inhibition to the purely excitatory network, whose synchrony requires a much stronger coupling, makes the cells switch to plateau bursting with smaller spikes which can be synchronized by the weaker excitatory coupling. The blue (dark) synchronization region, bounded by curves $E1$ and $E2$, corresponds to synchronized bursting and indicates a synergistic balance between the excitation and inhibition. Overly strong inhibition destroys synchrony (through boundary $E2$) and leads to antiphase bursting, as expected [Fig. 2(d)].

The key component of the synergistic mechanism is the ability of inhibition to induce plateau bursting via the disappearance of a homoclinic bifurcation (HB) in the two-dimensional (2D) fast subsystem ($\mu = 0$) of system (2) that governs the type of synchronized bursting. Figure 3 illustrates the bifurcation mechanism of this transition from square-wave to plateau bursting. According to the Izhikevich classification [5], square-wave bursting corresponds to fold-homoclinic bursting where the burst termination is determined by a homoclinic loop to a saddle in the fast subsystem. Increasing synaptic coupling in the self-coupled system (2), whether excitatory or inhibitory, eventually leads to the disappearance of this homoclinic bifurcation and induces plateau bursting (fold-fold bursting in the Izhikevich classification). This can be achieved by strong excitation [see Fig. 2(b)] or by weaker inhibition [see Fig. 2(c)]. The fast $(x,y)$ subsystem of the self-coupled system (2) has the nullcline $z = h(x) \equiv -\alpha x^2 - x^3 + g_{\rm exc}(V_{\rm exc} - x)\Gamma(x) + g_{\rm inh}(V_{\rm inh} - x)\Gamma(x)$. The excitatory (inhibitory) coupling moves the nullcline $z = h(x)$ to the right (left) (see Fig. 3). Remarkably, a small shift of the right branch of $z = h(x)$ towards the synaptic threshold $x = \Theta_{\rm s}$ (to the left) caused by weaker inhibition effectively decreases the divergence inside the limit cycle of the fast system, forming the spiking manifold. This causes the limit cycle to shrink in size and makes the homoclinic orbit disappear. At the same time, a much larger amount of excitation is necessary to shift the right branch of $z = h(x)$ to a far-right region where the divergence is small enough for a similar switch from square-wave to plateau bursting via the disappearance of the homoclinic orbit (see the HB curve in Fig. 2(top); the curve is calculated using the bifurcation analysis software CONTENT [33]).

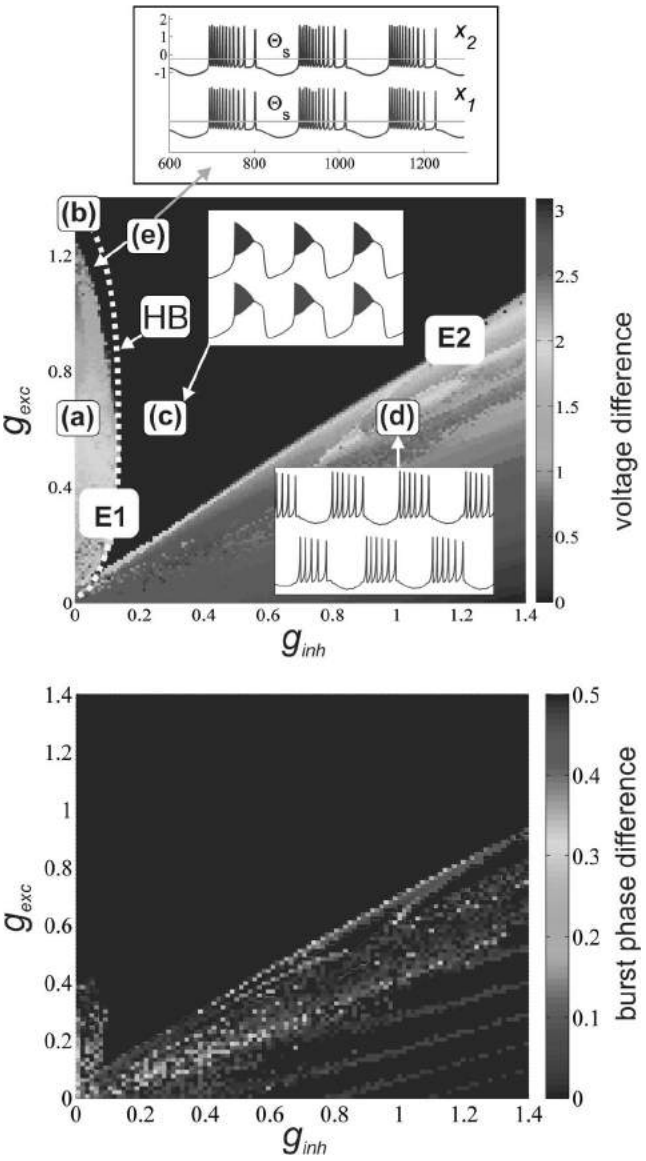


FIG. 2. (Color online) Synchronization in the two-cell network (1) as a function of excitation ($g_{\rm exc}$) and inhibiton ($g_{\rm inh}$). Top panel: The color bar indicates the voltage difference $|x_1 - x_2|$, averaged over the last three bursting periods. The blue (dark) zone (c) corresponds to the zero voltage difference (complete synchronization), appearing from random initial conditions. Observe the effect when a small increase of inhibition from 0 dramatically lowers the synchronization threshold from 1.28 to 0.11. Note that the inhibition desynchronizes the cells in the absence of excitation ($g_{\rm exc} = 0$), independently from the coupling strength and initial conditions. Bifurcation curve HB (white dotted line) corresponds to the transition to synchronized plateau bursting. Bottom panel: Burst synchronization. The color bar indicates the phase difference between the bursts, $\Delta\phi = \phi_1 - \phi_2$, averaged over the last three bursting periods. The normalized phase $0 \leqslant \phi_i \leqslant 1$ of the $i$th bursting cell ($i = 1,2$) is initiated and reset every cycle at the beginning of the burst. The normalized phase difference $\Delta\phi$ ranges from 0 [burst synchrony, blue (dark gray) color] to 0.5 [antiphase bursting, red (light gray) color]. Notice a similar effect of burst synchronization, induced by repulsive inhibition.

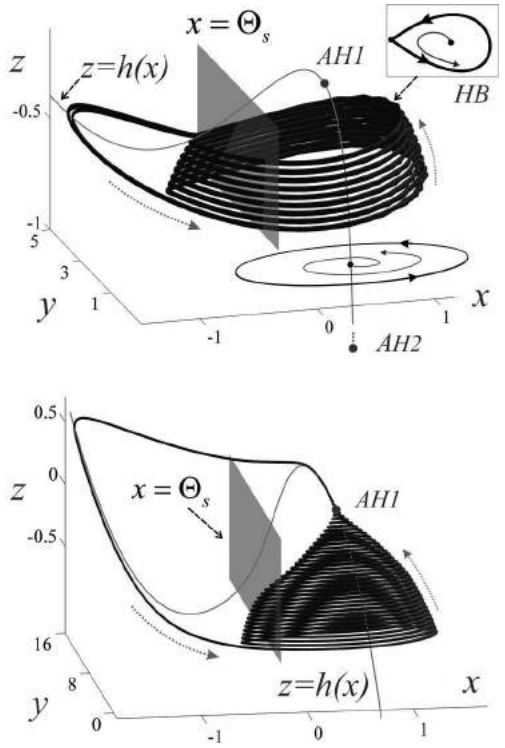


FIG. 3. (Color online) Transition from square-wave to plateau bursting in the self-coupled system (2), controlling the type of synchronous bursting. Top: Square-wave burster in the uncoupled network (1). The right branch of the fast nullcline $z = h(x)$ contains two points $AH1$ and $AH2$ corresponding to supercritical Andronov-Hopf bifurcations. A limit cycle of the fast system ($\mu = 0$) is born from the Andronov-Hopf bifurcation $AH2$ and grows in size as $z$ increases. This family of limit cycles constitutes the spiking manifold which terminates at the homoclininc bifurcation HB of the saddle point of the fast system, located on the middle branch of $z = h(x)$. The red (dotted) curve schematically indicates the route for bursting trajectories. The plane $x = \Theta_s$ displays the synaptic threshold. Bottom: Plateau bursting induced by the combination of excitatory and inhibitory coupling ($g_{\rm exc} = 0.6$ and $g_{\rm inh} = 0.25$), corresponding to point (c) in Fig. 2. The added inhibition leads to the disappearance of the homoclinic bifurcation such that the spiking manifold extends further up and disappears as the limit cycle shrinks to zero amplitude and disappears via the reverse Andronov-Hopf bifurcation $AH1$.

Switching to synchronized plateau bursting also shifts the plateau part of the burst to the right from the synaptic threshold (see Fig. 3). Due to the choice of the synaptic sigmoidal function $\Gamma(x_j)$ in (1), the coupling between the cells remains continuous during this part of the burst while being pulsatile in the first half of the burst where the spikes cross the synaptic threshold $\Theta_s$. This might not be the case in cortical networks where the coupling is always pulsatile. Figure 2(e) indicates the region between the stability boundary $E1$, corresponding to the onset of induced synchrony, and the HB curve, indicating the transition to synchronized plateau bursting. This region corresponds to synchronized square-wave bursting where all the spikes cross the synaptic threshold $\Theta_s$, making the coupling pulsatile for all times. We have also performed numerical simulations of the network (1) with the sigmoidal function $\Gamma(x_j)$, replaced by the Heaviside function $H(x_j)$, representing realistic fast pulse coupling. The obtained stability diagrams are similar to the ones of Fig. 2 with a slight expansion of the left stability zone bounded by $E1$ along the $x$ and $y$ axes, up to the synchronization coupling threshold $g_{\rm exc} = 1.35$ in the purely excitatory network [cf. the synchronization threshold $g_{\rm exc} = 1.28$ in the network with the sigmoidal function $\Gamma(x_j)$]. This increase in the coupling comes from the fact that the Heaviside-type pulse coupling has a weaker impact, compared to the sigmoidal-type coupling. As a result, larger values of $g_{\rm exc}$ and $g_{\rm inh}$ are required to achieve the same effect.

## IV. STABILITY MECHANISM

### A. Two-cell network

To explain the synchronization mechanism, we use the stability equations for the infinitesimal transverse perturbations $\xi_{12} = x_1 - x_2$, $\eta_{12} = y_1 - y_2$, $\zeta_{12} = z_1 - z_2$ [9]:

$$\begin{aligned} \dot{\xi}_{12} &= (2ax - 3x^2)\xi_{12} - \eta_{12} - \zeta_{12} - \Omega(x)\,\xi_{12}, \\ \dot{\eta}_{12} &= 2(a+\alpha)x\xi_{12} - \eta_{12}, \quad \dot{\zeta}_{12} = \mu(b\xi_{12} - \zeta_{12}), \end{aligned} \tag{3}$$

where $\Omega(x) = S_1 + S_2$, $S_1 = (g_{\rm exc} + g_{\rm inh})\Gamma(x)$, and $S_2 = [g_{\rm exc}(V_{\rm exc} - x) + g_{\rm inh}(V_{\rm inh} - x)]\Gamma'_x(x)$. Here $x(t)$ is the synchronous solution defined via the self-coupled system (2) and $\Gamma'_x(x)$ is the partial derivative of $\Gamma(x)$ with respect to $x$. The stability of the zero equilibrium $\{\xi_{12} = 0, \eta_{12} = 0, \zeta_{12} = 0\}$ of the linearized system (3) corresponds to the stability of the synchronous solution in the original network. The function $\Omega(x)$ represents the contribution of the excitatory and inhibitory coupling; it favors the stability of synchronization when it becomes positive and has a destabilizing impact when it is negative [9]. More specifically, the coupling term $-\Omega(x)\,\xi_{12}$ aims at stabilizing the zero equilibrium of system (3) when it is positive and tends to destabilize the zero equilibrium when it is negative.

The two terms $S_1$ and $S_2$, composing $\Omega(x)$, heavily depend on whether the voltage $x(t)$ exceeds the synaptic threshold $\Theta_s$. The first term $S_1$ contains the sigmoidal synaptic function $\Gamma(x)$ and becomes significant for $x(t) \geqslant \Theta_s$. Once turned on, the term $S_1 > 0$ makes $\Omega(x) > 0$ for $x(t) \geqslant \Theta_s$ (see Fig. 4) and favors the stability for both excitatory and inhibitory coupling as $g_{\rm exc} + g_{\rm inh} > 0$.

The second term, $S_2$, can change sign; the term due to the excitatory coupling $g_{\rm exc}(V_{\rm exc} - x)$ is positive and therefore attractive, whereas the inhibitory one $g_{\rm inh}(V_{\rm inh} - x)$ is negative and repulsive. It contains the derivative $\Gamma'_x(x)$ which has a peak around $\Theta_s$ and rapidly decaying tails [in the case of the Heaviside function $H(x_i)$, $\Gamma'_x(x)$ turns into the $\delta$ function]. Therefore, the term $S_2$ switches and remains on for the values of $x$, close to the threshold $\Theta_s$ when the spikes cross the threshold. It becomes decisive for the overall sign of $\Omega(x)$ in a region around the threshold $\Theta_s$, giving a distinct bell shape to $\Omega(x)$ (see Fig. 4).

When $x(t)$ drops below the threshold $\Theta_s$, the cells are practically uncoupled. Our Lyapunov-function-based analysis of synchronization in excitatory networks [9,10] suggests that the spikes are the most unstable part of the synchronous

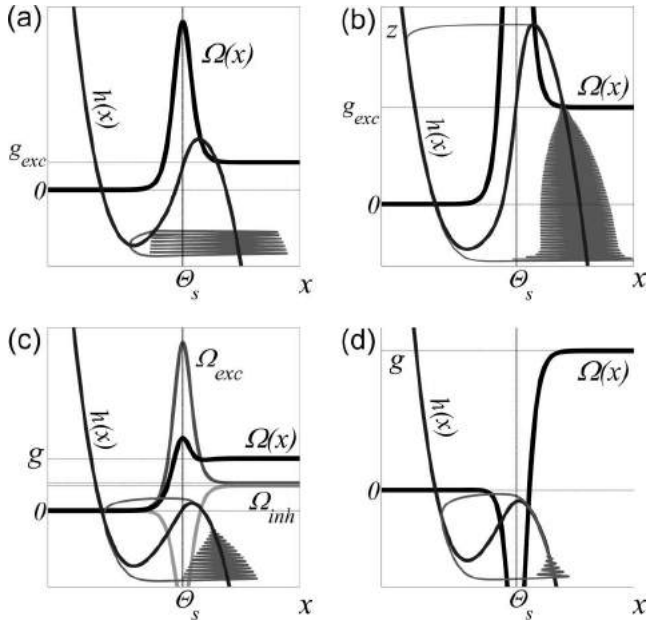


FIG. 4. (Color online) Stability function $\Omega(x)$ for synchronized bursting. Panels (a), (b), (c), and (d) correspond to the points (a), (b), (c), and (d) in Fig. 2. (a) $g_{\rm exc} = 0.6$, $g_{\rm inh} = 0$: Unstable square-wave synchronous bursting [brown (gray)] and the fast nullcline $h(x)$ of the self-coupled system, together with $\Omega(x)$ superimposed on its own scale. The impact of $\Omega(x)$ subthreshold where the coupling is insignificant (to the left from the threshold $\Theta_s$). (b) $g_{\rm exc} = 1.28$, $g_{\rm inh} = 0$: The increased excitation makes the impact of $\Omega(x)$ stronger; more importantly, it changes the type of synchronous bursting. Notice that the spikes have shifted to the right and moved to the region where the strong coupling is present. (c) $g_{\rm exc} = 0.6$, $g_{\rm inh} = 0.25$: The red (upper) curve represents the contribution of the excitatory coupling $\Omega_{\rm exc} = g_{\rm exc}\Gamma(x) + g_{\rm exc}(V_{\rm exc} - x)\Gamma'_x(x)$, the green (light gray) curve corresponds to that of the inhibitory coupling $\Omega_{\rm inh} = g_{\rm inh}\Gamma(x) + g_{\rm inh}(V_{\rm inh} - x)\Gamma'_x(x)$, and the thick black line indicates the combined curve $\Omega(x) = \Omega_{\rm exc} + \Omega_{\rm inh}$. Adding the inhibition decreases the impact of $\Omega(x)$ [cf. with (a) where $\Omega(x)$ equals $\Omega_{\rm exc}$ in (c)]. At the same time, it induces plateau bursting, with the spikes in the region above the threshold, where the coupling is sufficiently strong to synchronize them. (d) $g_{\rm exc} = 0.6$, $g_{\rm inh} = 0.9$: Strong inhibition destabilizes synchronous plateau bursting. $\Omega(x)$ has a drop in the region, covering the upper knee of the nullcline. As a result, the cells diverge when slowly crawling up this part of the nullcline. Note that synchronous plateau bursting of the self-coupled system is unstable and does not represent the dynamics observed in the network; the cells become locked into antiphase square-wave bursting [cf. Fig. 2(d)].

solution such that their stabilization via the synaptic coupling yields complete synchronization. The above-threshold part of the synchronous solution lies in the stability zone as the coupling function $\Omega(x) > 0$ for any combination of $g_{\rm exc}$ and $g_{\rm inh}$. Therefore, this part of the solution can be stabilized by making the coupling stronger. At the same time, the subthreshold part of the synchronous spikes is difficult to stabilize as the contribution of the term $S_2$ rapidly decays to zero below from the threshold. Moreover, only excitatory coupling can stabilize the synchronous trajectory in the subthreshold region as it yields the positive peak of the bell-shaped curve $\Omega(x)$ [see Fig. 4(a)]. The addition of inhibition lowers this peak and can make it negative [see Fig. 4(d)], making the region around the threshold less stable. Figures 4(a) and 4(b) show that increasing $\Omega(x)$ (via increasing $g_{\rm exc}$) induces synchrony in the purely excitatory network. However, it requires fairly strong excitation to stabilize the synchronous solution, especially its subthreshold part. Figure 4(c) demonstrates that adding the inhibition has a twofold effect. It lowers the stabilizing impact of $\Omega(x)$ around and below the synaptic threshold; however, it helps switching the type of synchronous bursting via (2), making the spikes shorter and moving them towards the stability region, controlled by the synchronizing term $S_1$. Increasing inhibition typically switches synchronous square-wave bursting to plateau bursting which places the spikes of synchronous bursting into the stability (above-threshold) region that can be, in turn, effectively stabilized by the excitatory coupling via $S_1$. Therefore, the combination of $g_{\rm exc} + g_{\rm inh}$ synergistically induces synchronized bursting within a wide region of parameters $g_{\rm exc}$ and $g_{\rm inh}$. Its right stability boundary $E2$ (cf. Fig. 2) corresponds to synchrony loss and is defined by the mutual arrangements between the graphs of $\Omega(x)$ and the nullcline $h(x)$ [Fig. 4(d)]. This happens when the upper knee of $h(x)$ falls inside the instability zone where $\Omega(x)$ is negative [cf. Fig. 4(d)]. The Appendix contains an additional argument for predicting the slope of boundary $E2$. This estimate $g_{\rm exc} = 0.78\, g_{\rm inh}$ (see the Appendix) coincides remarkably well with the numerically calculated boundary $E2$ in Fig. 2.

It is important to restate that the dynamics and type of synchronous bursting $x(t)$ are controlled by the self-coupled system (2) and depend on both $g_{\rm exc}$ and $g_{\rm inh}$. This property allows the inhibition to induce plateau bursting in the self-coupled system (2). The synchronous bursting observed in the self-coupled system (2) does not necessarily represent the emergent network dynamics. This synchronous solution can be unstable, especially when $g_{\rm inh}$ is overly strong as in Fig. 4(d). Therefore, the network generates a different stable rhythm; this is typically antiphase square-wave bursting as in Fig. 2(d) (cf. the two insets for consistency).

While the onset of inhibition-induced synchronization is typically governed by the transition from square-wave to plateau bursting, the addition of inhibition can also induce synchronized square-wave bursting in a smaller region of parameters [Fig. 2(e)]. However, the synchronization mechanism is essentially the same; the inhibition decreases the subthreshold part of the spikes, without changing the type of bursting, and thus facilitates synchronization, although fairly strong excitation is required, making the synergistic effect less pronounced.

### B. Larger networks: The scaling laws

The discovered inhibition-induced synchronization phenomenon is also present in larger networks of square-wave bursters (1). We demonstrate that the structure of the added inhibitory connections is not important and only the number of inhibitory inputs controls the onset of synchronization, independent from all other details of their network topology. In the context of complex dynamical networks, this unexpected result indicates the drastically different roles of network topology in synchronization of linearly [28,29] and synaptically coupled networks with attractive and repulsive

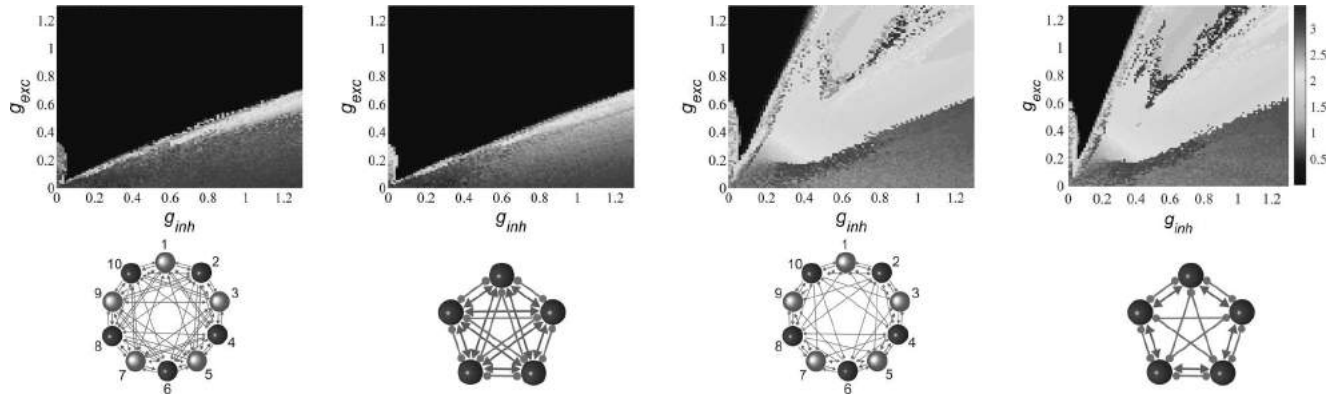


FIG. 5. (Color online) Stability diagrams for network synchronization, similarly to that of Fig. 2. The color bar indicates the mean voltage difference $\sum_{i=1}^{n-1}\sum_{j>i}^{n}\frac{2}{n(n-1)}(x_i - x_j)$, calculated and averaged over the last three bursting periods. Notice the nearly identical diagrams for pairs of 10-cell irregular and 5-cell regular networks with $k_{\rm exc} = 4$ and $k_{\rm inh} = 4$ (left pair) and $k_{\rm exc} = 2$ and $k_{\rm inh} = 4$ (right pair). Excitatory (inhibitory) connections are depicted by arrows (circles). Excitatory (inhibitory) neurons in the 10-cell irregular networks [with only outgoing excitatory (inhibitory) connections] are denoted by light (dark) circles. The height and width of the left instability zone, adjacent to the $g_{\rm exc}$ axis and corresponding to desynchronized square-wave bursting, are inversely proportional to $k_{\rm exc}$ and $k_{\rm inh}$, respectively (also compare with Fig. 2).

connections. Figure 5 shows that the size of the left desynchronization zone, bounded by the $g_{\rm exc}$ axis and boundary $E1$ (cf. Fig. 2), scales down vertically and horizontally by $k_{\rm exc}$ and $k_{\rm inh}$ times, respectively. As a result, the stability boundaries $E1$ for the onset of synchrony are nearly identical for networks of different sizes and topologies, provided that $k_{\rm exc}$ and $k_{\rm inh}$ are uniform for each cell. In support of this claim, we have analyzed a series of different regular and random networks (1) with uniform numbers of excitatory ($k_{\rm exc}$) and inhibitory ($k_{\rm inh}$) synapses per neuron. For all simulated networks, numerical results are consistent with the scaling law above. Figure 5 demonstrates two representative pairs of networks yielding the largest and smallest regions of inhibition-induced synchronization for all possible network topologies (1) with the given number of excitatory and inhibitory inputs. Figure 6 summarizes the numerical simulations of different networks with different topologies and shows how the synchronization effect of added inhibition scales with the size of the network.

To show that the scaling laws carry over to larger networks with random coupling matrices, we have simulated a 100-cell random network where each cell receives four excitatory $k_{\rm exc} = 4$ and four inhibitory $k_{\rm inh} = 4$ connections (Fig. 7). The network consists of 80 excitatory and 20 inhibitory cells such that the excitatory (inhibitory) cells only have excitatory (inhibitory) outgoing connections, thereby abiding by Dale's law. Both excitatory and inhibitory coupling strengths are mismatched by adding $\Delta g_{ij} q$ to $g_{\rm exc}$ and $g_{\rm inh}$ for each existing connection $(i, j)$. The mismatch parameter $\Delta g_{ij}$ is expressed as a percentage of $g_{\rm exc}$ and $g_{\rm inh}$ and kept equal to 5%; the values of the parameter $q$ are chosen randomly from the interval $(-1, 1)$ for each excitatory and inhibitory connection $(i, j)$, yielding a 10% maximum mismatch. The stability diagram supports the scaling law and has a structure similar to the two left diagrams in Fig. 5, all corresponding to different network topologies with the uniform number of connections $k_{\rm exc} = 4$ and $k_{\rm inh} = 4$.

To target realistic biological networks with nonuniform numbers of excitatory and inhibitory inputs per neuron, we have simulated a 100-cell network, similar to that of Fig. 7, but with an *average* number of inputs $k_{\rm exc} = 4$ and $k_{\rm inh} = 4$. This heterogeneous network has been generated from the network topology of Fig. 7 with $k_{\rm exc} = 4$, $k_{\rm inh} = 4$, and nonmismatched $g_{\rm exc}$ and $g_{\rm inh}$ by randomly choosing a pair of cells and changing their in-degrees of the excitatory and inhibitory inputs by subtracting one incoming connection of each type from one cell and adding these connections to the other cell. As a result, one half of the cells have $k_{\rm exc} = 3$ and $k_{\rm inh} = 3$, while the other half have $k_{\rm exc} = 5$ and $k_{\rm inh} = 5$, yielding the average $k_{\rm exc} = 4$ and $k_{\rm inh} = 4$. This effective mismatch between the overall strength of the incoming connections to each neuron is larger than the 10% maximum mismatch used in the previous example (Fig. 7); however, the stability diagram for approximate synchronization is quite similar to Fig. 7, except for the appearance of a more irregular structure of the synchronization stability zone due to the increased coupling mismatch. Increasing the heterogeneity mismatch between the connections even further shall eventually make approximate spike synchronization impossible; however, we expect induced burst synchronization to persist.

To explain the scaling law, we shall return to the transversal variational equations (3) written for $n-1$ difference variables $\xi_{ij} = x_i - x_j$, $\eta_{ij} = y_i - y_j$, $\zeta_{ij} = z_i - z_j$, and $i, j = 1, \ldots, n$. The equations for the purely excitatory networks were given in Ref. [9] where an analog of the master stability function [27] for synaptically coupled networks (1) was used to analyze the stability of the most unstable transverse mode. Unfortunately, the master stability function cannot be applied to mixed excitatory-inhibitory networks in general as it requires simultaneous diagonalization of both the excitatory ($C$) and inhibitory ($D$) connectivity matrices. This is impossible in general unless the two matrices commute [34]. In the latter case, the stability equation for the most unstable transverse synchronous mode is Eq. (3) with a new stability function $\Omega^{\rm new}(x) = (k_{\rm exc} g_{\rm exc} + k_{\rm inh} g_{\rm inh})\Gamma(x) - g_{\rm exc}(V_{\rm exc} - x)\Gamma'_x(x)(k_{\rm exc} + \gamma_2^{\rm exc}) - g_{\rm inh}(V_{\rm inh} - x)\Gamma'_x(x)(k_{\rm inh} + \gamma_2^{\rm inh})$, where $\gamma_2^{\rm exc}$ and $\gamma_2^{\rm inh}$ are the second largest eigenvalues of the (commuting) Laplacian connectivity matrices for the

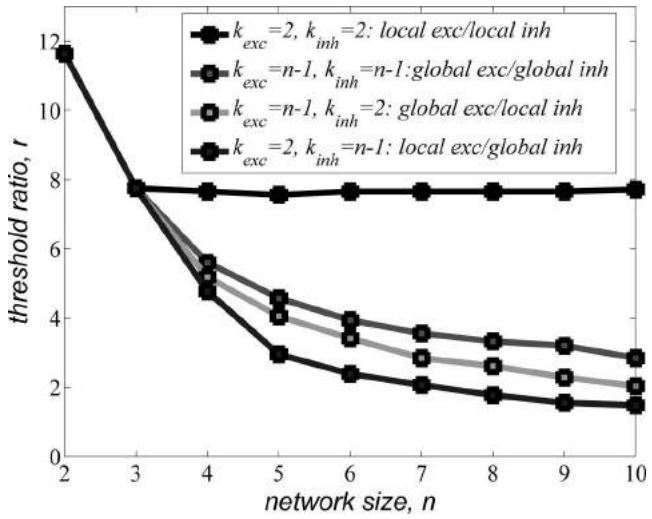


FIG. 6. (Color online) Ratio of the synchronization threshold in an excitatory network without inhibition and the minimum synchronization threshold achieved by adding inhibition, as a function of the network size $n$, for different values of $k_{\rm exc}$ and $k_{\rm inh}$. The ratio of the synchronization threshold reduction, induced by added inhibition is as large as 12 for the two-cell network (compare with Fig. 2). The four curves represent four types of network topology: rings of cells with local excitatory and inhibitory connections ($k_{\rm exc}=2$ and $k_{\rm inh}=2$); all-to-all networks with both global excitatory and inhibitory connections ($k_{\rm exc}=n-1$ and $k_{\rm inh}=n-1$); networks with global excitatory and local inhibitory connections ($k_{\rm exc}=n-1$ and $k_{\rm inh}=2$); and rings of cells with local excitatory and all-to-all inhibitory connections ($k_{\rm exc}=2$ and $k_{\rm inh}=n-1$). Notice that the addition of global inhibition to a locally coupled excitatory network (local excitation-global inhibition) yields the smallest reduction in the synchronization threshold for $n>3$ (lowest line) and therefore has the worst synchronization properties. At the same time, the addition of local inhibition to the same locally coupled excitatory network yields the highest reduction ratio for $n>3$ (top line) and indicates a nontrivial synergistic effect of the combined inhibitory and excitatory topologies. Also observe that global inhibition promotes synchronization more significantly than local inhibition when added to a globally coupled excitatory network, as the global excitation-global inhibition configuration has a higher synchronization threshold reduction ratio (second line from the top) compared to that of the global excitation-local inhibition configuration (third line from the top).

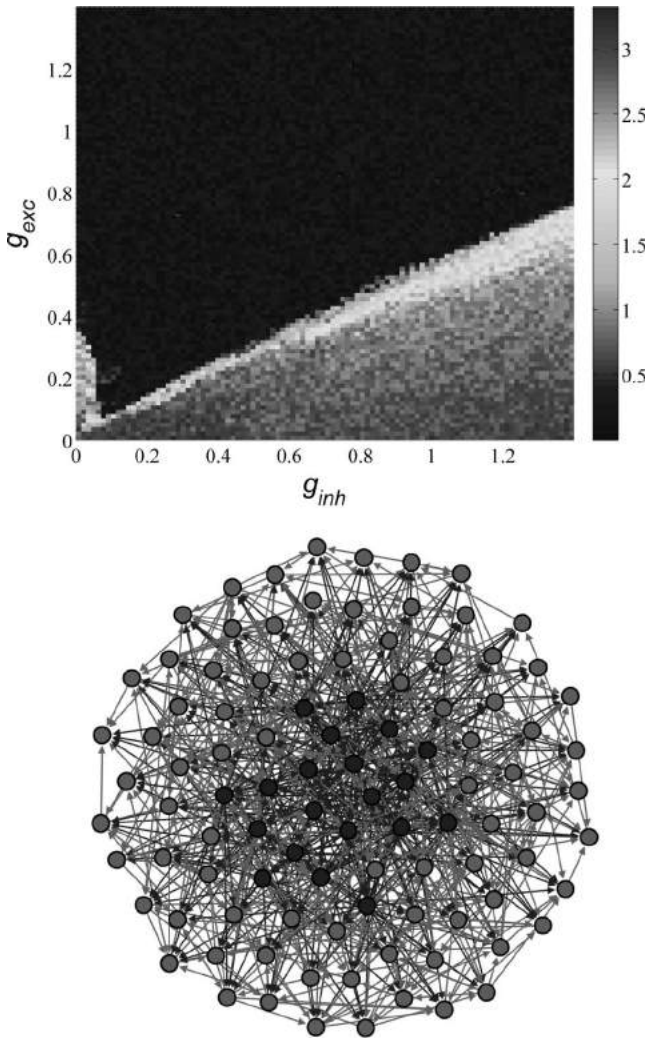


FIG. 7. (Color online) Top: Induced synchronization in a 100-cell randomly generated network with uniform $k_{\rm exc}=4$ and $k_{\rm inh}=4$. Bottom: The network has 80 excitatory [red (light gray)] and 20 inhibitory [blue (dark gray)] cells. The excitatory connections are marked by red (light gray) arrowed lines; the inhibitory coupling is indicated by blue (dark gray) arrows. Both excitatory and inhibitory coupling strengths are heterogeneous, with randomly distributed mismatch up to 10%. The color bar indicates the mean voltage difference as in Fig. 5. The stability diagram is similar to those of the two left diagrams in Fig. 5, corresponding to the 5- and 10-cell networks with $k_{\rm exc}=4$ and $k_{\rm inh}=4$. Complete spike synchronization is impossible in this mismatched network; however, an approximate synchronization with small voltage differences (offsets between the spikes) is robustly present. Various shades of blue (black) and the nonhomogeneous structure of the synchronization stability zone correspond to slight voltage offsets due to the parameter mismatch.

excitatory and inhibitory networks, $C^L=C-k_{\rm exc}\mathbf{I}$ and $D^L=D-k_{\rm inh}\mathbf{I}$, respectively. The first term in $\Omega^{\rm new}(x)$ accounts for the number and strength of excitatory and inhibitory inputs. The last two terms, containing the partial derivative $\Gamma_x'$ and the networks structure via $\gamma_2^{\rm exc}$ and $\gamma_2^{\rm inh}$, only matter for the stability or instability of synchronization in the region of $x(t)$, close to the synaptic threshold $\Theta_s$, similarly to the two-cell network case. The shift of the nullcline $h(x)$ and switching from square-wave to synchronous plateau bursting are governed by $k_{\rm exc}g_{\rm exc}$ and $k_{\rm inh}g_{\rm inh}$ via the self-coupled system (2). As a result, the spikes of the synchronous bursting solution leave the bell-shaped zone [similarly to Fig. 4(c)] such that the contribution of the last two terms in $\Omega^{\rm new}(x)$ becomes insignificant for synchronization. This yields the scaling law when the minimum strength of added inhibition $g_{\rm inh}^*$, sufficient to induce plateau-bursting synchrony, is inversely proportional to $k_{\rm inh}$, regardless of the network size and structure (compare, for example, $g_{\rm inh}^*\approx 0.14$ in the two-cell network of Fig. 2 and $g_{\rm inh}^*\approx 0.035=0.14/4$ in the networks of Fig. 5 with $k_{\rm inh}=4$, all calculated at the level $g_{\rm exc}=0.2$). Notice that the five-cell networks of Fig. 5 correspond to the commuting excitatory and inhibitory

connectivity matrices: global excitation–global inhibition and local excitation–global inhibition. In the case where the connectivity matrices do not commute (the 10-cell networks of Fig. 5 and the 100-cell network of Fig. 7), the eigenvalues of the connectivity matrices cannot be used and the stability function $\Omega^{\text{new}}(x)$ cannot be derived. A modification of the connection graph method [35] that uses graph theoretical reasoning instead of the spectrum of the connectivity matrices can be used to write down a set of similar stability functions. However, the stability argument is essentially the same, the induced synchronization is governed by the transition to plateau bursting that is, in turn, controlled by the self-coupled system. Consequently, the same scaling law for the inverse dependence of the induced synchronization threshold on $g_{\text{exc}}$ and $k_{\text{inh}}$ also holds for realistic noncommuting coupling configurations. Our results also indicate that the loss of stable synchrony via the right (inclined) boundary (similarly to boundary $E2$ in Fig. 2) is governed by a simple condition $g_{\text{exc}} = \alpha \frac{k_{\text{inh}}}{k_{\text{exc}}} g_{\text{inh}}$, where $\alpha$ is a scaling factor, uniform for different topologies with the same ratio $k_{\text{inh}}/k_{\text{exc}}$. As in the two-cell network yielding the slope $g_{\text{exc}} = 0.78\, g_{\text{inh}}$, this condition is determined by the shift of the nullcline $h(x)$ such that the upper knee of $h(x)$ moves close to the synaptic threshold $\Theta_s$ and falls into the instability zone [as in Fig. 4(c)].

## V. CONCLUSIONS

We have discovered the synergistic effect of combined attractive excitation and repulsive inhibition in promoting bursting synchrony. Remarkably, the addition of the inhibitory coupling lowers the synchronization threshold much more significantly than strengthening the present excitatory connections. The effect is generic and observed in other Hodgkin-Huxley-type models of square-wave bursting cells [36], including Sherman models [37] with $V_{\text{exc}} = 10$ mV, $V_{\text{inh}} = -75$ mV, $\Theta_s = -40$ mV [36]. The effect is also independent of the choice of the synaptic interaction model, ranging from the instantaneous pulsatile coupling to a fast dynamical synapse [15]. While fast nondelayed inhibition can lead to the coexistence of synchronous and antiphase bursting in some bursting models [18] when the coupling is weak, typically comparable to the small intrinsic parameter of the individual neuron, a significant synergistic effect is only observed in a range of coupling where the inhibition is purely repulsive and strong to change the type of bursting. Our preliminary results show that inhibition also promotes burst synchrony in realistic networks with a highly heterogeneous structure of connections, where spike or approximate synchrony is impossible. Our study has potential implications for understanding the emergence of abnormal synchrony in epileptic brain networks. An epileptic patient is normally (i.e., except for during a seizure) in a desynchronized state which might correspond to the instability region to the left of the $E1$ border in Fig. 2. Our results suggest that promoting presumably desynchronizing inhibition in an attempt to prevent the patient's seizures can have a counterproductive effect and induce abnormal synchronous firing in the excitatory-inhibitory brain network. Brain networks have been also shown to evolve their functional topology during epileptic seizures [2]. In light of this, our results on the role of network connectivity, identifying network topologies with the highest and lowest resilience of abnormal synchronized bursting, can give insights into how seizures self-terminate and into how to control epileptic networks. Outside neuroscience, negative pairwise repulsive interactions were previously shown to have a positive effect on synchronization in *linearly* coupled networks, where negative interactions by themselves tend to destabilize synchronous states but can compensate for other instabilities [29]. However, this intriguing phenomenon, where the structure of negative connections heavily affects the synchronization, conceptually differs from the one reported in this study. Apart from synchronization, a counterintuitive role of inhibition was reported in Ref. [38], demonstrating that the addition of inhibitory nodes to an excitatory network of 1D discrete-time oscillators causes self-sustaining dynamics.

## ACKNOWLEDGMENTS

This work was supported by the U.S. Army Research Office under Grant No. W911NF-15-1-0267, the National Science Foundation (USA) under Grant No. DMS-1009744, and GSU Brains & Behavior program. R.R. acknowledges support from the GSU Brains & Behavior program. We thank Russell Jeter for helpful discussions. We are also grateful to the anonymous reviewers for their constructive suggestions.

## APPENDIX: SLOPE OF SYNCHRONY LOSS BOUNDARY $E2$

This Appendix provides additional support for explaining synchrony loss, caused by overly strong inhibition via the stability boundary $E2$ (see Fig. 2). In addition to the stability argument based on the variational equations (see Sec. IV), we use a more straightforward approach to predict the slope of the boundary $E2$ in the two-cell network.

The network equations (1) can be written for the two-cell network as follows:

$$\begin{aligned} \dot{x}_i &= a x_i^2 - x_i^3 - y_i - z_i + g_{\text{exc}}(V_{\text{exc}} - x_i)\Gamma(x_j) \\ &\quad + g_{\text{inh}}(V_{\text{inh}} - x_i)\Gamma(x_j), \\ \dot{y}_i &= (a+\alpha)x_i^2 - y_i, \\ \dot{z}_i &= \mu(b x_i + c - z_i),\ i,j = 1,2. \end{aligned} \tag{A1}$$

Note that the combined action of two excitatory and inhibitory synapses essentially amounts to that of one synaptic connection with strength $g_{\text{syn}}$ and synaptic reversal potential $E_{\text{syn}}$. The corresponding system reads:

$$\begin{aligned} \dot{x}_i &= a x_i^2 - x_i^3 - y_i - z_i + g_{\text{syn}}(E_{\text{syn}} - x_i)\Gamma(x_j), \\ \dot{y}_i &= (a+\alpha)x_i^2 - y_i, \\ \dot{z}_i &= \mu(b x_i + c - z_i), \quad i,j = 1,2. \end{aligned} \tag{A2}$$

The synaptic reversal potential $E_{\text{syn}}$ changes in the range $[-2, 2]$, allowing us to vary the type of the connection from purely inhibitory when $E_{\text{syn}} = -2 < x_i$ for all $x_i(t)$, to purely excitatory when $E_{\text{syn}} = 2 > x_i(t)$. In this setting, changing the coupling strengths $g_{\text{exc}}$ and $g_{\text{inh}}$ in the network (A1) with fixed $V_{\text{exc}} = 2$ and $V_{\text{inh}} = -2$ is equivalent to changing the values of $g_{\text{syn}}$ and $E_{\text{syn}}$ in the network (A2). Figure 8 shows robust synchronization in an interval of $g_{\text{syn}}$ and $E_{\text{syn}}$.

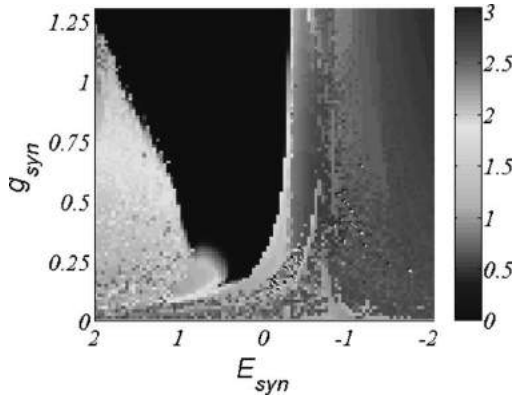


FIG. 8. (Color online) Role of $E_{\rm syn}$ in synchronization of the two-cell network (A1). The stability diagram and color coding are similar to those of Fig. 2. Decreasing the reversal potential $E_{\rm syn}$ from 2 first dramatically lowers the synchronization threshold. Dropping $E_{\rm syn}$ below $-0.25$ makes the connection essentially inhibitory such that synchronization cannot be achieved for any value of $g_{\rm syn}$: Note the vertically rising stability boundary around $E_{\rm syn} = -0.25$.

Here the left stability boundary, indicating the drop of the synchronization threshold from 1.28 with decreasing $E_{\rm syn}$ from 2, corresponds to the boundary $E1$ in Fig. 2. The vertical stability boundary for synchrony loss at $E_{\rm syn} = -0.25$ corresponds to the boundary $E2$ in Fig. 2. The origin of this almost vertically rising boundary, starting roughly at $E_{\rm syn} = -0.25$ is of no mystery if one realizes that this is also the synaptic threshold $\Theta_s = -0.25$. It is not a coincidence that these two values appear equal. Note that the synaptic connection becomes purely inhibitory when $x_i(t)$ exceeds the reversal potential $E_{\rm syn}$. Therefore, the part of the synchronous solution lying above $E_{\rm syn}$ (mainly, the above-threshold part of the spikes) cannot be robustly stabilized. At the same time, when $x_i(t)$ is below $E_{\rm syn}$, the synapse is excitatory. As Fig. 2 suggests, when $E_{\rm syn}$ is chosen as low as $\Theta_s$, the excitatory action of the synapse is nonexistent as the synapse is practically off below the synaptic threshold $\Theta_s$.

This is the key observation for predicting the slope of the stability boundary $E2$ in the original network (1). We return to the network (1) and notice that for the overall impact of the excitatory and inhibitory connections to be robustly synchronizing, the overall input to the $i$-th cell, $g_{\rm exc}(V_{\rm exc} - x_i)\Gamma(x_j) - g_{\rm inh}(V_{\rm inh} - x_i)\Gamma(x_j)$, must remain positive. Rewriting this condition yields $\frac{g_{\rm exc}V_{\rm exc}+g_{\rm inh}V_{\rm inh}}{g_{\rm exc}+g_{\rm inh}} - x_j > 0$, as $\Gamma(x_j) \geqslant 0$. Notice that the first term plays a role of the reversal potential $E_{\rm syn}$ in the network (A2). Therefore, according to Fig. 8, $\frac{g_{\rm exc}V_{\rm exc}+g_{\rm inh}V_{\rm inh}}{g_{\rm exc}+g_{\rm inh}}$ cannot exceed $E_{\rm syn} \approx \Theta_s = -0.25$ for synchronization to remain stable. This yields the following condition on the stability boundary $g_{\rm exc} = \frac{\Theta_s - V_{\rm inh}}{V_{\rm exc} - \Theta_s} g_{\rm inh}$, written in terms of the parameters of the original network (1). Plugging in the values of the parameters $V_{\rm inh} = -2$, $V_{\rm exc} = 2$, and $\Theta_s = -0.25$, one gets $g_{\rm exc} = 0.78 g_{\rm inh}$. This condition predicts the slope of the boundary line $E2$ remarkably well. This argument also carries over to larger networks and supports the scaling law for synchrony loss: $g_{\rm exc} = \alpha \frac{k_{\rm inh}}{k_{\rm exc}} g_{\rm inh}$.


[1] T. I. Netoff and S. J. Schiff, J. Neurosci. **22**, 7297 (2002); K. Schindler, C. E. Elger, and K. Lehnertz, Clin. Neurophysiol. **118**, 1955 (2007).

[2] K. Lehnertz, G. Ansmann, S. Bialonski, H. Dickten, C. Geier, and S. Porz, Physica D (Amsterdam) **267**, 7 (2014).

[3] J. Rinzel, *Lecture Notes in Biomathematics*, Vol. 71 (Springer-Verlag, Berlin, 1987), pp. 251–291.

[4] D. Terman, SIAM J. Appl. Math. **51**, 1418 (1991); R. Bertram, M. J. Butte, T. Kiemel, and A. Sherman, Bull. Math. Biol. **57**, 413 (1995); V. N. Belykh, I. Belykh, M. Colding-Joergensen, and E. Mosekilde, Eur. Phys. J. E **3**, 205 (2000); A. Shilnikov and G. Cymbalyuk, Phys. Rev. Lett. **94**, 048101 (2005); A. L. Shilnikov and M. L. Kolomiets, Int. J. Bifurcat. Chaos **18**, 2141 (2008).

[5] E. M. Izhikevich, Int. J. Bifurcat. Chaos **10**, 1171 (2000).

[6] F. Frohlich and M. Bazhenov, Phys. Rev. E **74**, 031922 (2006).

[7] E. M. Izhikevich, SIAM Rev. **43**, 315 (2001).

[8] M. Dhamala, V. K. Jirsa, and M. Ding, Phys. Rev. Lett. **92**, 028101 (2004).

[9] I. Belykh, E. de Lange, and M. Hasler, Phys. Rev. Lett. **94**, 188101 (2005).

[10] I. Belykh and M. Hasler, Chaos **21**, 016106 (2011).

[11] D. Somers and N. Kopell, Biol. Cybern. **68**, 393 (1993).

[12] N. Kopell and G. B. Ermentrout, Proc. Natl. Acad. Sci. USA **101**, 15482 (2004).

[13] X.-J. Wang and J. Rinzel, Neural, Comput. **4**, 84 (1992).

[14] C. van Vreeswijk, L. F. Abbott, and G. Bard Ermentrout, J. Comput. Neurosci. **1**, 313 (1994).

[15] D. Golomb and J. Rinzel, Phys. Rev. E **48**, 4810 (1993); D. Terman, N. Kopell, and A. Bose, Physica D (Amsterdam) **117**, 241 (1998); R. C. Elson, A. I. Selverston, H. D. I. Abarbanel, and M. I. Rabinovich, J. Neurophysiol. **88**, 1166 (2002); U. Ernst, K. Pawelzik, and T. Geisel, Phys. Rev. Lett. **74**, 1570 (1995); S. Sadeghi and A. Valizadeh, J. Comput. Neuroscience **36**, 55 (2014); F. S. Matias, P. V. Carelli, C. R. Mirasso, and M. Copelli, Phys. Rev. E **84**, 021922 (2011).

[16] J. Rubin and D. Terman, SIAM J. Appl. Dynam. Syst. **1**, 146 (2002).

[17] J. Rubin and D. Terman, Neural Comput. **12**, 597 (2000).

[18] S. Jalil, I. Belykh, and A. Shilnikov, Phys. Rev. E **81**, 045201(R) (2010); **85**, 036214 (2012).

[19] I. Belykh and A. Shilnikov, Phys. Rev. Lett. **101**, 078102 (2008).

[20] C. C. Canavier, D. A. Baxter, J. W. Clark, and J. H. Byrne, Biol. Cybern. **80**, 87 (1999).

[21] A. Shilnikov, R. Gordon, and I. Belykh, Chaos **18**, 037120 (2008).

[22] J. Wojcik, R. Clewley, and A. Shilnikov, Phys. Rev. E **83**, 056209 (2011); J. Wojcik, R. Clewley, J. Schwabedal, and A. Shilnikov, PLoS ONE **9**, e92918 (2014).

[23] R. Vicente, L. L. Gollo, C. R. Mirasso, I. Fischer, and G. Pipa, Proc. Natl. Acad. Sci. USA **105**, 17157 (2008).
[24] L. L. Gollo, C. Mirasso, O. Sporns, and M. Breakspear, PLoS Comput. Biol. **10**, e1003548 (2014).
[25] K. Tsaneva-Atanasova, H. Osinga, T. Riel, and A. Sherman, J. Theor. Biol. **264**, 1133 (2010).
[26] G. P. Krishnan and M. Bazhenov, J. Neurosci. **31**, 8870 (2011).
[27] L. M. Pecora and T. L. Carroll, Phys. Rev. Lett. **80**, 2109 (1998); L. M. Pecora, Phys. Rev. E **58**, 347 (1998).
[28] I. Leyva, I. Sendina-Nadal, J. A. Almendral, and M. A. F. Sanjuań, Phys. Rev. E **74**, 056112 (2006).
[29] T. Nishikawa and A. E. Motter, Proc. Natl. Acad. Sci. USA **107**, 10342 (2010).
[30] M. Ren, Y. Yoshimura, N. Takada, S. Horibe, and Y. Komatsu, Science **316**, 758 (2007).
[31] B. W. Connors and S. J. Cruikshank, Nat. Neurosci. **10**, 808 (2007).
[32] H. H. Dale, Proc. Royal Soc. Med. **28**, 319 (1934).
[33] CONTENT is availabe on its main developer's webpage (Yu. A. Kuznetsov), http://www.staff.science.uu.nl/∼kouzn101/CONTENT.
[34] F. Sorrentino, New J. Phys. **14**, 033035 (2012); D. Irving and F. Sorrentino, Phys. Rev. E **86**, 056102 (2012).
[35] V. N. Belykh, I. V. Belykh, and M. Hasler, Physica D (Amsterdam) **195**, 159 (2004).
[36] R. Reimbayev and I. Belykh, Int. J. Bifurcat. Chaos **24**, 1440013 (2014).
[37] A. Sherman, Bull. Math. Biol. **56**, 811 (1994).
[38] D. B. Larremore, W. L. Shew, E. Ott, F. Sorrentino, and J. G. Restrepo, Phys. Rev. Lett. **112**, 138103 (2014).